29th Congress of the International Council of the Aeronautical Sciences
St. Petersburg, Russia; September 7-12, 2014

MODEL OF THE UNSTEADY AERODYNAMIC CHARACTERISTICS AT HIGH AOA WITH NONLINEAR DEPENDENCY IN ANGULAR RATE

D.I. Ignatyev, A.N. Khrabrov
Central Aerohydrodynamic Institute, TsAGI, Russia

Keywords: *unsteady aerodynamic characteristics, modeling, pitch moment, wind tunnel tests*

Abstract

Experimental study of unsteady aerodynamic characteristics of a passenger aircraft over an extended angle-of-attack range was carried out using a series of forced-oscillation tests. Strong nonlinear effects, namely, an influence of oscillation frequency on aerodynamic derivatives and hysteresises with multiple self-intersections, were observed. The experimental results enable an influence of a pitch rate on unsteady pitch moment to be analyzed. A model of unsteady aerodynamic characteristics with Nonlinear Dependency in Angular Rate (NDAR) describing the main dynamic effects observed in the experiment was developed. The proposed model is compared with linear, state-space and neural network models.

1 Introduction

Recent studies showed that loss of control in flight is one of the main threats to civil aviation safety [1]. This fact stimulates investigations of flight dynamic and development of flight simulators for pilot training in the extended flight envelope [2, 3]. For successive solving of such problems more comprehensive mathematical models of aerodynamics in the extended flight envelope are required.

Simulation of unsteady aerodynamic characteristics at high angles of attack is complicated with their nonlinear behavior depending on motion prehistory. For the aircraft with high-aspect-ratio wing determining physical effect at high angles of attack is a dynamics of flow separation and its interference with a flow over a total aircraft configuration. Delay of the flow separation/reattachment with variation of angles of attack and sideslip leads to nonlinear variation of aerodynamic coefficients.

The aerodynamic forces and moments are usually represented in terms of aerodynamic derivatives in engineering applications of flight dynamic problems [6, 7]. For example, for small disturbance motion about a small trim incidence α_0, the pitch moment coefficient is supposed to be represented as the linear terms of Taylor series expansion in the motion parameters

$$C_m = C_m(\alpha_0) + C_{m_\alpha}(\alpha - \alpha_0) + C_{m_q}(q\bar{c}/2V) + C_{m_{\dot{\alpha}}}(\dot{\alpha}\bar{c}/2V) \quad (1)$$

This method can be successfully applied at the normal flight conditions. In the stall conditions the aerodynamic characteristics are strongly nonlinear and application of this approach can lead to significant errors.

General technique of modeling the unsteady aerodynamic characteristics uses the nonlinear indicial functions [5]. To develop the aerodynamics model based on the nonlinear indicial functions a large amount of unsteady aerodynamic data should be used. Nevertheless, it requires a set of serious simplifications when applied to real problems, so that final mathematical models are formulated in a simple form of first-order linear differential equations [6].

The state-space model [7] takes into account delays of flow separation and reattachment for an airfoil. Aerodynamic

characteristics of a full-aircraft configuration can be separated into linear non-delaying and nonlinear delaying components while using this approach [8-9]. Ordinary differential equations are used for modeling the dynamics of the nonlinear components of aerodynamic characteristics. These equations contain time constants corresponding to the characteristic times of the flow separation and reattachment. These time constants are identified using the dynamic wind-tunnel test results. Such approach enables the dependences of aerodynamic derivatives on frequency and amplitude of oscillations, and aerodynamic hysteresis to be modeled quite precisely. At the same time, application of the state-space model in an arbitrary case is complicated because of non-formalized and expert-based procedure of a model structure identification.

Neural network (NN) approach can be considered as an alternative. NN have been shown recently to be a formal and an effective tool for modeling of nonlinear unsteady aerodynamics regardless of the aircraft configurations [9-12]. Such an active application of neural networks is mainly connected with their universal approximation properties, which enable the neural networks to be used for an arbitrary aircraft without significant simplifying assumptions. The main disadvantages of NN approach are "Black-box" principle and difficulties with determination of the application limits.

This study aimed at developing of a unsteady pitching moment model with Nonlinear Dependency In Angular Rate (NDAR). Experimental study of unsteady aerodynamic characteristics of passenger aircraft using forced oscillation tests were carried out. Influence of the pitch rate on the unsteady pitch moment coefficient is analyzed. The simulation results obtained with proposed technique are compared with conventional, state-space and NN techniques.

2 Experiment

Experimental studies of unsteady aerodynamic characteristics of a passenger aircraft configuration were conducted in TsAGI low-speed wind tunnel T-103. The aircraft model is low-wing monoplane with high aspect ratio wing, a conventional tail unit with a single vertical stabilizer and two wing-mounted engines. Corresponding Reynolds number is $\mathrm{Re} = 1.8 \cdot 10^5$. The aircraft model in the wind tunnel is shown in Fig.1.

Fig.1. Wind tunnel dynamic tests of passenger aircraft.

Conventional technique for obtaining unsteady aerodynamic data is the forced harmonic oscillations

$$\alpha = \alpha_0 + \Delta\alpha \sin(2\pi f t), \qquad (2)$$

where α_0 is a mean angle of attack, $\Delta\alpha$ is an oscillation amplitude, f is an oscillation frequency.

The present experimental investigations were conducted in three stages. Static characteristics were obtained at the first stage. Dynamic tests, forced small-amplitude oscillations, with amplitude $\Delta\alpha = 3$ deg, frequences from 0.5 to 2 Hz, and velocity $V = 25$ m/s in the angle-of-attack range from -5 to 60 deg were conducted in the second stage. The small-amplitude tests were aimed at determining of aerodynamic derivatives $C_{m\alpha}$ and $C_{mq} + C_{m\dot{\alpha}}$. Fig. 2 shows the obtained results.

At the last stage, studying of dynamic effects of flow separation/reattachment was conducted using forced large-amplitude oscillations [13]. The amplitudes were

$\Delta\alpha = 5 \div 20$ deg, the frequencies were $f = 0.2 \div 1.5$ Hz, and the flow velocities were $V = 12.5 \div 25$ m/s.

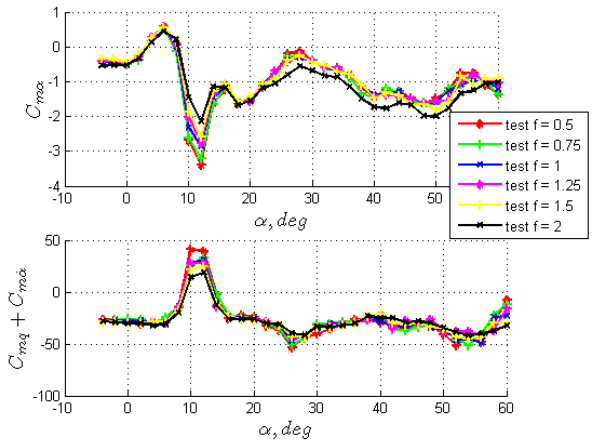

Fig. 2. Aerodynamic derivatives obtained using small –amplitude tests

Conducted small-amplitude tests revealed the incidence region $\alpha \approx 9 \div 16$ of nonlinear variation of unsteady derivatives (Fig. 2). In this region damping changes sign and becames positive, that leads to aircraft dynamic instability in pitch. Examination of the figure gives also a conclusion that positive damping decreases as oscillation frequency increases (Fig. 2).

The large-amplitude tests revealed that oscillation frequency was also significant for the total pitch momemt coefficient. The results of large-amplitude ($\Delta\alpha = 10, 20$ deg) tests are given in Fig. 3.

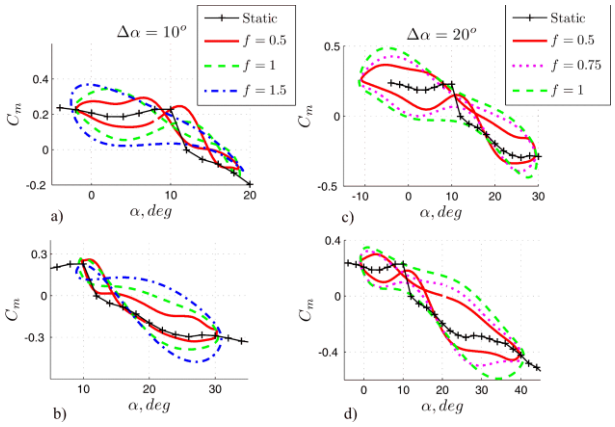

Fig 3. Pitch moment coefficient hysteresis loops obtained using large-amplitude oscillation test: frequency effects

For a set of test cases the hysteresys loops have self-intersections at the angle-of-attack range $\alpha \approx 9 \div 16$, where the positive damping was revealed for the aerodynamic derivatives. The test cases (3a, 3c, and 3d) show that the self-intersection loops decrease and further vanish at all as oscillation frequency increases. The hysteresys loop in case 3b decrease but does not vanish. The explanation of this fact will be given further.

The influence of oscillation amplitude on the unsteady pitch moment was also studied in the experiment. The pitch moment dependencies obtained at different amplitudes ($\Delta\alpha = 10, 20$ deg) for the frequency f =1 Hz are given in Fig. 4. The hysteresis self-intersection loops are observed for smaller amplitude of oscillation ($\Delta\alpha = 10$ deg) and are not observed for the higher amplitude ($\Delta\alpha = 20$ deg) at the same frequency.

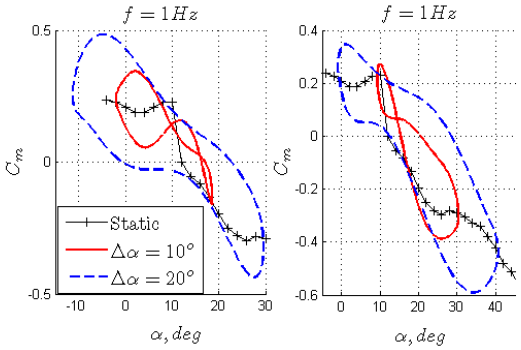

Fig. 4. Pitch moment coefficient hysteresis loops obtained using large-amplitude oscillation test: amplitude effects

The observed amplitude and frequency effects at the longitudinal motion can be joined. The experimental results analysis leads to conclusion that increase of both the frequency and the amplitude of oscillations decreases the positive damping. These phenomena could be generalized through introducing nonlinear dependency of unsteady pitch moment on dimensionless angular rate where the frequency and the amplitude are included naturally:

$$\bar{q} = \frac{q \cdot \bar{c}}{2V} = \frac{\pi \cdot f \cdot \Delta\alpha \cdot \cos(2\pi \cdot f \cdot t) \cdot \bar{c}}{V}$$

The complex of unsteady aerodynamic derivatives $C_{mq} + C_{m\dot{\alpha}}$ plotted against dimensionless rate $\bar{q}_{\max} = \frac{\pi \cdot f \cdot \Delta\alpha \cdot \bar{c}}{V}$ is given

in Fig. 5. The figure corresponds to angle-of-attack $\alpha = 15$ deg that lies in the angle of attack region of nonlinear variation of pitch moment. This fact enables the qualitative analysis of the positive damping dependence on angular rate to be carried out. The presented data obtained from various harmonic tests (2) carried out with various combinations of parameters $\Delta\alpha, f, V$. Particularly, for the amplitude $\Delta\alpha = 3$ deg the frequencies f were from 0.5 to 2 Hz and the velocity was $V = 25$ m/s. For the amplitude $\Delta\alpha = 5$ the frequencies f were from 0.2 to 1.5 Hz and the velocity was from 12.5 to 25 m/s. Markers on the figure show experimental values and a solid line shows approximating spline curve.

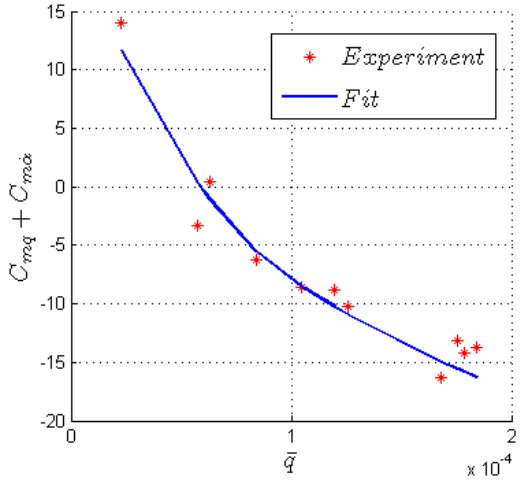

Fig. 5. Complex of damping derivatives $C_{mq} + C_{m\dot{\alpha}}$ versus dimensionless angular rate.

Presented plot clearly demonstrates that the positive damping is a single-valued function of angular rate in the incidence region of flow separation regardless of the oscillation frequency and amplitude.

It can be concluded from the figure that positive damping is a decreasing function of angular rate. This fact explains the obtained experimental dependencies (Fig. 2, 3, 4), namely, the frequency increasing leads to positive damping diminishing (Fig. 2), and the frequency and amplitude increasing leads to vanishing of self-intersection loops of pitch moment hysteresis (Fig. 3, 4). Additionally, the fact that self-intersection loop does not vanish in Fig 3b can be also understood. In this case the model has small angular rate in the region of positive damping.

3 NDAR Model

The obtained experimental results enable the model of unsteady pitch moment coefficient at high angles of attack to be developed. The model precision increases as the width of investigated range of angular rate broadens. For identification of the model the data obtained using large-amplitude oscillations were used since quite wide ranges of rates $\bar{q}$ and angles of attack α are available during these tests. Phase trajectories are shown in Fig. 6 for illustration of the possible states.

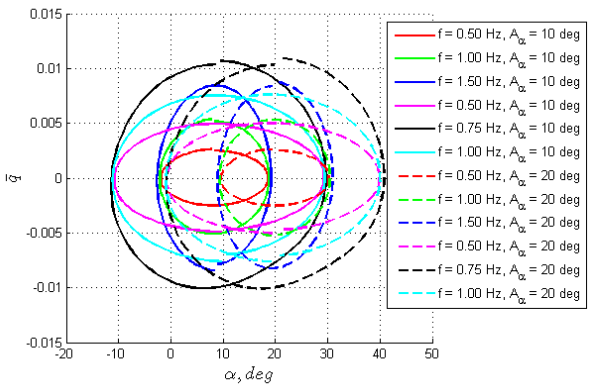

Fig. 6. Phase portraits of the large-amplitude tests.

Based on the experimental data a two-dimension array $C_m(\alpha, \bar{q})$ was formed. The array data are given graphically in Fig. 7.

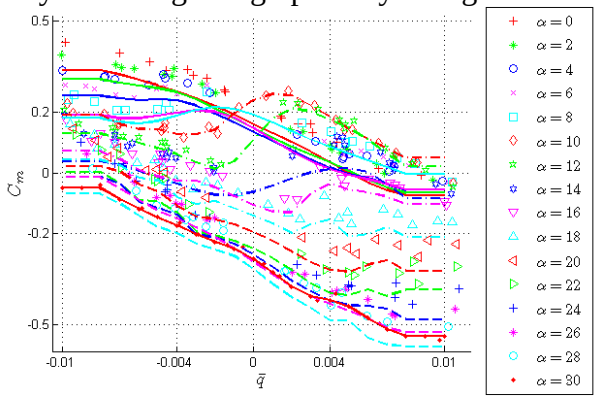

Fig. 7. Pitch moment coefficient versus angular rate.

Dependency of the pitch moment coefficient C_m on the angular rate $\bar{q}$ is practically linear at $\alpha \approx 0 \div 4$ deg, the nonlinear

behavior develops in the angle of attack range $\alpha \approx 6 \div 8$. A strong nonlinear behavior is in the range $\alpha \approx 10 \div 14$, namely, the curve slope changes the sign and at the small $\bar{q}$ derivative $C_{mq} + C_{m\dot{\alpha}}$ becomes positive, the positive damping is observed. With further increase of angle of attack the dependency of $C_{mq} + C_{m\dot{\alpha}}$ on $\bar{q}$ again becomes linear, positive damping vanishes.

The pitch moment simulating at arbitrarily values of $\alpha, \bar{q}$ is carried out through a two-dimensional spline interpolation of array $C_m(\alpha, \bar{q})$. Conventional look-up table of the pitch moment coefficient simplifies solving of the flight dynamics problems.

4 Simulation Results And Comparison With Other Models

4.1 NDAR Simulation

At the beginning let us consider the results of simulation using the NDAR model.

Simulation of the pitch moment coefficient obtained during the large-amplitude oscillations is presented in Fig. 8. The experimental results and simulation using conventional technique (1) are also plotted in the same figure for comparison.

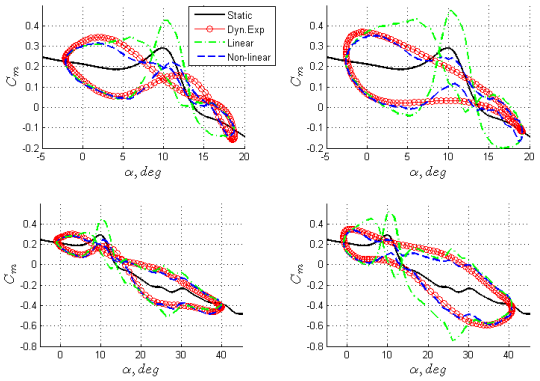

Fig. 8. Simulation of the pitch moment coefficient during large-amplitude oscillations.

One can conclude from the figure that the proposed technique describes the results observed in experiment. Otherwise the conventional technique fails to simulate unsteady pitch moment in the angle of attack range, in which flow separation develops.

The large-amplitude tests were used for developing of the data array $C_m(\alpha, \bar{q})$ but the proposed technique can also used for describing the small-amplitude test results (Fig. 9).

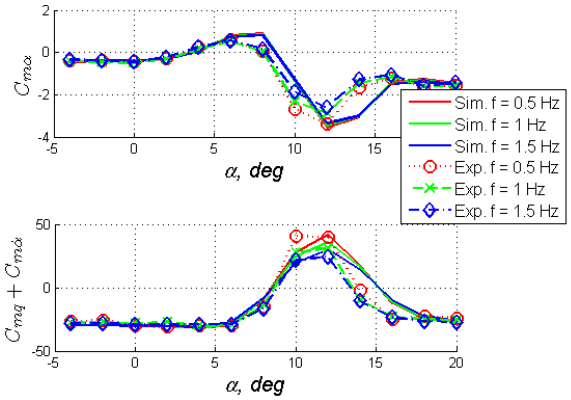

Fig. 9. Simulation of the unsteady aerodynamic derivatives of the pitch moment coefficient.

Let us compare the discussed model with a state-space [6] and a NN [12] models that were developed also in the present study. Firstly, the description of the state-space model for the given aircraft configuration is presented below.

4.2 State-Space Model

Within the state-space approach the total pitch moment is divided into two components, namely,

$$C_m = C_{mk} + C_{mq}\bar{q}\,, \qquad (3)$$

where $C_{mq}(\alpha)$ is dynamic derivative.

The component C_{mk} is divided into linear $C_{m\,lin}$ and nonlinear $C_{m\,nonlin}$ parts, which are determined by attached and separated flow

$$C_{mk} = C_{m\,lin} + C_{m\,nonlin}\,, \qquad (4)$$

Equation (4) hold true both for steady and unsteady conditions. $C_{m\,lin}(\alpha)$ is a linear function of the angle of attack. The following differential equation for $C_{m\,nonlin}$ is used in unsteady case

$$\tau_1 \dot{C}_{m\,nonlin} + C_{m\,nonlin} = C_{m\,nonlin\,St}(\alpha - \tau_2 \dot{\alpha})\,, \qquad (5)$$

here τ_1, τ_2 is characteristic time constants. Function $C_{m\,nonlin\,St}(\alpha)$ in the right side of the equation (5) is a steady dependency of the nonlinear component of the pitch moment in angle of attack and can be represented as difference between the steady total pitch moment coefficient $C_{mSt}(\alpha)$ and the linear part $C_{m\,lin}(\alpha)$, namely,

$$C_{m\,nonlin\,St}(\alpha) = C_{mSt}(\alpha) - C_{m\,lin}(\alpha). \qquad (6)$$

The components $C_{mSt}(\alpha)$, $C_{m\,lin}(\alpha)$, $C_{m\,nonlin\,St}(\alpha)$ are plotted in Fig. 10 for illustration.

The time constants τ_1, τ_2, and derivative $C_{mq}(\alpha)$ of the mathematical model are identified from the experiment results and were approximated using spline curves (Fig. 10).

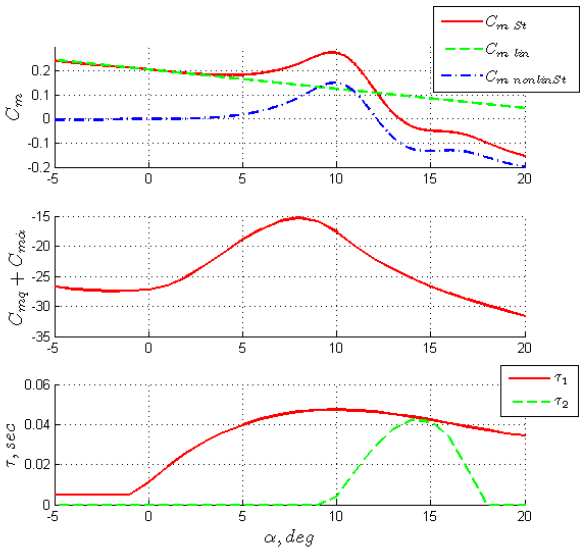

Fig. 10. State-space model.

4.3 Neural Network

A neural network can be considered as a directed graph with weighted connections (Fig. 11). Elementary processors, which are called artificial neurons, are the nodes of the graph [14]. Each neuron k receives "input signals'' $(e_i)_{i=1,n}$ from other neurons or from the network input nodes. Having received a set of the input signals, the neuron multiplies each signal by the corresponding weight coefficient w_{ik}, summarizes the obtained multiplications, and corrects the sum on corresponding bias b_k. The result of summation is mapped through nonlinear activation function f_k.

In such a way, the neuron maps the input signal $(e_i)_{i=1,n}$ into output signal y_k as follows:

$$y_k = f_k\left(\sum_i w_{ik} e_i + b_k\right)$$

A neural network architecture in the general case consists of several neuron layers. The first layer neurons receive input signals, distribute them between neurons of the second layer. The signal processing is carried out in the inner ('hidden') layers of the NN: the signal is processed firstly by the first 'hidden' layer, then by the second 'hidden' and so on. The last layer does not process the signal but yields the output signals to the interpreter or user. Usually, each output signal of the i layer is presented to the input of all the neurons of the i+1 layer. Additionally, the feedback connections between layers can be used. NNs with feedback connections (recurrent NN) are usually used for modeling of consequence of states and were applied for simulation of unsteady aerodynamic characteristics in flight dynamics problems [10, 12]

A recurrent NN of NARX (Nonlinear AutoRegressive model with eXogenous variables) architecture [17] with one hidden layer was used in the present paper. NN configuration is represented in Fig. 11. For modeling variable y at time t the state vector $\mathbf{x}(t)$ and a series of its former values $\mathbf{x}(t-1), \mathbf{x}(t-2) \ldots \mathbf{x}(t-D_{in})$ are fed into the neural network. The values of variable $y(t-1), y(t-2) \ldots y(t-D_{out})$ modeled by the NN on the previous steps are also used. The resulting neural network model can be presented in the following form

$$y(t) = M(\mathbf{x}(t), \mathbf{x}(t-1), \ldots, \mathbf{x}(t-D_{in}), y(t-1), \ldots, y(t-D_{out}))$$

where M is the function of neural network operations.

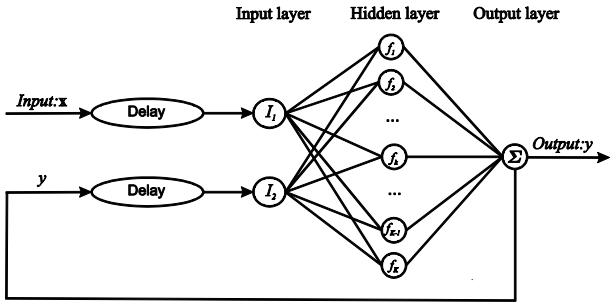

Fig. 11. NN architecture

The NN in the present study has 12 neurons in the hidden layer. Activation function of the neurons was a sigmoid $f_k(x) = \frac{1}{1+e^{-x}}$.

Experimental data, which were used to train the NN, consisted of the oscillation cases corresponding to different amplitudes and frequencies of oscillation. Evolutions of the pitch moment coefficient and kinematic parameters during each oscillating case were discretized in time into 128 steps. Small-amplitude oscillation cases were 78, large-amplitude oscillation cases were 12. The training patterns were composed of the target data, which were the records of pitch moment coefficient $C_m(i), C_m(i-1)$ at steps i, i-1, together with the input vector. The input vector included the angle of attack $\alpha(i)$ and pitch rate $q(i)$ at the i–th step, and the motion parameters $\alpha(i-1), \alpha(i-2)$, $q(i-1), q(i-2)$ at previous steps i-1, i-2. A special regularization technique increasing model generalization at the heteroscedastic data was used while NN training [16].

4.4 Model comparison

The model performances were tested quantitatively by calculating the errors obtained for the simulated pitch moment coefficient C_m for large-amplitude oscillations. The error measure is the mean square error divided by the entire range Δy of the measured value y^{test}:

$$err_i = \frac{\sqrt{\frac{1}{N_i - 1}\sum_{j=1}^{N_i}(y_j^{test} - y_j^{sim})^2}}{\Delta y}$$

The results are given in Table 1.

Model	Error, %
Nolinear NDAR	3.09
Conventional Linear	7.74
State-space	3.94
Neural Network	2.84

Firstly, the table proves that the linear model error is quite high for description of the unsteady aerodynamics at high angles of attack as compared to the nonlinear models. Secondly, errors of all nonlinear models are approximately on the same level. NDAR model error is lesser than state-space model and higher then NN model.

5 Conclusion

The analysis of the frequency and amplitude influencies on the unsteady pitch moment coefficient obtained at the forced oscillation wind tunnel tests is carried out. The nonlinear behavior of unsteady pitch moment at high angles of attack, namely, complex hysteresises with self-intersection loops and dependencies of aerodynamic derivatives on oscillation frequency, is shown to be significantly determined by dimensionless pitch rate.

The model of unsteady aerodynamic characteristics at high angles of attack with Nonlinear Dependency in Angular Rate (NDAR) is proposed in the paper. This dependency is presented as spline-approximation of the look-up table $C_m(\alpha, \bar{q})$ developed using the data from large-amplitude oscillations.

A quantitative comparison of the NDAR model of unsteady pitch moment with linear, state-space and NN models is carried out. The error of large-amplitude test simulation is calculated for each of the model. All nonlinear models have approximately the same level of errors that is good enough for flight dynamics problems. At the same time, NDAR model

features, namely, simplicity and conventional structure in the form of look-up table, facilitate application of it in the engineering problems, for example, in the flight dynamics studying, control law design and real-time simulation with pilot in loop using flight simulators.

Acknowledgments

This work is partially supported by the Russian Foundation for Basic Research (no. 12-08-00679)

References

[1] Annual Safety Review 2011. *European Aviation Safety Agency* [online rept.], URL: https://www.easa.europa.eu/communications/docs/annual-safety-review/2011/EASA-Annual-Safety-Review-2011.pdf [cited 02 April 2014].

[2] Abramov N.B., Goman M.G., Khrabrov A.N., Kolesnikov E.N., Fucke L., Soemarwoto B., and Smaili H. Pushing Ahead - SUPRA Airplane Model for Upset Recovery. *AIAA Modeling and Simulation Technologies Conference*, Minneapolis, Minnesota, AIAA 2012-4631, 2012.

[3] Foster, J.V., Cunningham, K., Fremaux, Ch.M., Shah, G.H., Stewart, E.C., Rivers, R.A., Wilborn, J.E., Gato, W. Dynamics Modeling and Simulation of Large Transport Airplanes in Upset Conditions. *AIAA Atmospheric Flight Mechanics Conference and Exhibit*, San Francisco, California, AIAA-2005-5933, 15-18 August 2005.

[4] Bushgens, G. S. (ed.), *Aerodynamics, stability and controllability of supersonic aircraft*, Nauka, Fizmatlit, Moscow, 1998, 816 p. [In Russian].

[5] Tobak M., Schiff L. B. On the formulation of the aerodynamic characteristics in aircraft dynamic. *NASA TR R - 456*, Washington, D.C., 1976.

[6] Klein V., Noderer K.D. Modeling of Aircraft Unsteady Aerodynamic Characteristics. Part 1 - Postulated Models. *NASA Technical Memorandum* 109120, 1994.

[7] Goman, M.G., Khrabrov, A.N. Space Representation of Aerodynamic Characteristics of an Aircraft at High Angles Attack. *Journal of Aircraft*, Vol. 31, No 5, pp. 1109 - 1115, 1994.

[8] N.Abramov, M.Goman, D.Greenwell and A.Khrabrov. Two-Step Linear Regression Method for Identification of High Incidence Unsteady Aerodynamic Model. *AIAA Atmospheric Flight Mechanics Conference*, Montreal, Canada, 2001, Paper 2001-4080, 2001.

[9] Vinogradov Yu. A., Zhuk A.N., Kolinko K. A., Khrabrov A. N. Mathematical simulation of dynamic effects of unsteady aerodynamics due to canard flow separation delay. *TsAGI Science Journal*, Vol. 42, No. 5, pp. 655-668, 2011.

[10] Faller, W.E. and Schreck S.J. Unsteady Fluid Mechanics Applications of Neural Networks. *Journal of Aircraft*, Vol. 34, No. 1, pp. 48-55, 1997.

[11] Planckaert L. Model of Unsteady Aerodynamic Coefficients of a Delta Wing Aircraft at High Angles of Attack. *RTO AVT Symposium on "Advanced Flow Management: Part A – Vortex Flows and High Angle of Attack for Military Vehicles"*, Loen, Norway, RTO-MP-069(I), 38.1 - 38.11, 2001.

[12] Ignatyev D. I., Khrabrov A.N. Application of neural networks in the simulation of dynamic effects of canard aircraft aerodynamics. *TsAGI Science Journal*, Vol. 42, No. 6, 2011, pp. 817-828.

[13] Ignatyev D.I. Simulation of unsteady aerodynamic characteristics of aircraft at high angles of attack using neural networks. *5-th European Conference For Aeronautics And Space Sciences (EUCASS)* [CD-ROM], Munich, 2013.

[14] Zhuk A.N., Kolinko K. A., Miatov O. L. Khrabrov A.N. Technique of unsteady aerodynamic characteristic investigation at the flow separation using large-amplitude oscillations. *Uchenye zapiski TsAGI*, Vol. XXVII, No 3-4, 1996.

[15] Wasserman P. D., *Neural computing: Theory and Practice*. Van Nostrand Reinhold, New York, NY, USA, 1989, 230 p.

[16] Ignatyev, D.I., Khrabrov A.N. Neural network modeling of longitudinal aerodynamic characteristics of aircraft, *Informatsionnye tekhnologii*, No. 3, 2014, pp. 60-69 (in Russian).

[17] Beale M. H., Hagan M. T., Demuth H. B., "Neural Network Toolbox User's Guide" [online book], URL: http://www.mathworks.com/help/ [cited 02 April 2014]

6 Contact Author Email Address

mailto: d.ignatyev@mail.ru

Copyright Statement